

University of Nebraska - Lincoln

DigitalCommons@University of Nebraska - Lincoln

Xiao Cheng Zeng Publications

Published Research - Department of Chemistry

5-30-2006

Evidence of hollow golden cages

Satya S. Bulusu

University of Nebraska-Lincoln, sbulusu@iiti.ac.in

Xi Li

Rowland Institute at Harvard, li@rowland.harvard.edu

Lai-Sheng Wang

Washington State University & Pacific Northwest National Laboratory, ls.wang@pnl.gov

Xiao Cheng Zeng

University of Nebraska-Lincoln, xzeng1@unl.edu

Follow this and additional works at: <https://digitalcommons.unl.edu/chemzeng>

 Part of the [Chemistry Commons](#)

Bulusu, Satya S.; Li, Xi; Wang, Lai-Sheng; and Zeng, Xiao Cheng, "Evidence of hollow golden cages" (2006). *Xiao Cheng Zeng Publications*. 17.

<https://digitalcommons.unl.edu/chemzeng/17>

This Article is brought to you for free and open access by the Published Research - Department of Chemistry at DigitalCommons@University of Nebraska - Lincoln. It has been accepted for inclusion in Xiao Cheng Zeng Publications by an authorized administrator of DigitalCommons@University of Nebraska - Lincoln.

Evidence of hollow golden cages

Satya Bulusu*, Xi Li^{†‡§}, Lai-Sheng Wang^{†‡¶}, and Xiao Cheng Zeng^{*¶}

* Department of Chemistry and Center for Materials and Nanoscience, University of Nebraska, Lincoln, NE 68588;

[†] Department of Physics, Washington State University, 2710 University Drive, Richland, WA 99354; and

[‡] Chemical Sciences Division, Pacific Northwest National Laboratory, MS K8-88, P.O. Box 999, Richland, WA 99352

[¶] To whom correspondence may be addressed. E-mail: ls.wang@pnl.gov or xczen@phase2.unl.edu

[§] Present address: Rowland Institute at Harvard, 100 Edwin H. Land Boulevard, Cambridge, MA 02142

Author contributions: S.B., L.-S.W., and X.C.Z. designed research; S.B., X.L., L.-S.W., and X.C.Z. performed research; L.-S.W. contributed new reagents/analytic tools; S.B., X.L., L.-S.W., and X.C.Z. analyzed data; and L.-S.W. and X.C.Z. wrote the paper.

Edited by Benjamin Widom, Cornell University, Ithaca, NY, and approved April 7, 2006 (submitted January 2006)

Abstract – The fullerenes are the first “free-standing” elemental hollow cages identified by spectroscopy experiments and synthesized in the bulk. Here, we report experimental and theoretical evidence of hollow cages consisting of pure metal atoms, Au_n^- ($n = 16$ –18); to our knowledge, free-standing metal hollow cages have not been previously detected in the laboratory. These hollow golden cages (“bucky gold”) have an average diameter >5.5 Å, which can easily accommodate one guest atom inside.

Keywords – anion photoelectron spectroscopy, density functional calculation, hollow gold cages, lowest-energy clusters

Abbreviations – DFT, density-functional theory; PES, photoelectron spectroscopy; VDE, vertical detachment energy

The isolation and detection of carbon-free hollow cages have attracted much interest since the discovery (1) and synthesis (2) of the buckyball C_{60} and the higher fullerenes. Although “free-standing” inorganic cages have been synthesized (3), bare elemental metal cages have not been observed in nature or detected in the laboratory. Among metals, gold has some unique properties including the strong relativistic effects and aurophilic attraction (4). Recently, a fullerene-like hollow cage with 32 Au atoms was predicted to be highly stable (5, 6). However, photoelectron spectroscopy (PES) combined with theoretical calculations shows that at the relatively large size the overwhelming population of low-lying clusters for Au_{32}^- near room temperature appears to consist of only compact structures because of the entropic factor (7). Other, larger gold clusters with cage-like local minimum structures also have been suggested (8, 9), but none has been observed experimentally. Conversely, it has been established from both ion-mobility (10) and PES (11) experiments that the most stable anion gold clusters (Au_n^-) in the size range $n = 5$ –13 possess planar structures and that a structural transition from planar to three-dimensional (3D) structures occurs at $n = 14$. Beyond $n = 14$, previous global-minimum searches based on empirical potential functions of gold (12, 13) or semiempirical tight-binding models of gold (14) suggest that all low-lying isomers of gold clusters assume space-filling compact structures. Among the larger gold clusters, Au_{20} is the most interesting; it has been found to possess a pyramidal structure with tetrahedral symmetry just as carved out of the bulk face-centered cubic crystal (15).

Results and Discussion

To elucidate the structural transition from the planar Au at $n = 13$ to the pyramidal Au_{20} , we carried out a joint experimental PES and theoretical study on Au_n^- for $n = 15$ –19. The measured spectra (see *Methods* below) are shown in Fig. 1*A* with numerous well resolved features in the lower binding energy part, which are used to compare with theoretically simulated spectra (Fig. 1*B* and *C* and *Methods* below; see also Fig. 3, which is published as supporting information on the PNAS web site) with the candidate lowest-energy clusters (see Fig. 4, which is published as supporting information on the PNAS

web site). The vertical detachment energies (VDEs) (given by the location of the first major peak near the threshold) for this feature are given in Table 1, compared with the theoretical VDEs from the lowest-energy structures. Note that the threshold of the lowest-binding-energy feature in each spectrum (see Table 2, which is published as supporting information on the PNAS web site) defines the electron affinity of the neutral clusters.

The theoretically obtained top-10 lowest-energy structures (see *Methods*) are given in Fig. 4. Among these top-10 isomers, we selected those isomers within 0.2 eV ($1 \text{ eV} = 1.602 \times 10^{-19} \text{ J}$) from the lowest-energy isomer and simulated their photoelectron spectra (Figs. 1*B* and *C* and 3). We regard these selected isomers as the candidates for the lowest-energy structure owing to the intrinsic error bar (<0.2 eV) of density-functional theory (DFT) electronic energy calculations (16–18) and the basis-set effects. The number of candidate lowest-energy isomers ranges from one for Au_{19}^- (Fig. 4*E*) to five for Au_{15}^- (Fig. 4*A*) and Au_{16}^- (Fig. 4*B*), and six for Au_{17}^- (Fig. 4*C*) and Au_{18}^- (Fig. 4*D*).

Remarkably, we observed that all but a total of three candidate lowest-energy isomers of Au_{16}^- , Au_{17}^- , and Au_{18}^- are “hollow cages” with an empty interior space (Fig. 4*B*–*D*). The interior space (typically with length scale >5.5 Å) of these hollow cages can easily host a foreign atom. Among the five candidate lowest-energy structures of Au_{15}^- (Fig. 4*A*), Au_{15a}^- , Au_{15b}^- , and Au_{15d}^- are flat-cage structures, whereas Au_{15c}^- and Au_{15e}^- are pyramidal-like structures. Previous studies have shown that in stable gold clusters, gold atoms tend to have maximum coordination number of six, e.g., in the 2D planar structures of Au_9 – Au_{13} (10, 11) and in the pyramidal structure of Au_{20} (15). Hence, it is understandable that both the flat-cage and pyramidal-like structures are energetically competitive for the gold clusters within the size range Au_{14} to Au_{20} . Conversely, it is quite surprising that the hollow-cage structures dominate the low-lying population of Au_{16}^- to Au_{18}^- clusters. Specifically, at Au_{16}^- , only Au_{16e}^- (among the five candidate lowest-energy structures) has flat-cage structure whose interior length scale can be <5 Å (Fig. 4*B*). The isomer Au_{16a}^- can be viewed as a relaxed structure of the pyramidal Au_{20} with four missing corner atoms but maintains the tetrahedral symmetry of Au_{20} (15). At Au_{17}^- , only Au_{17c}^- among the six candidate lowest-energy structures has a flat-cage structure (Fig. 4*C*), whereas at Au_{18}^- , only Au_{18a}^- among the six candidate lowest-energy structures exhibits pyramidal-like (non-hollow-cage) structure (Fig. 4*D*). Note that Au_{17a}^- can be viewed as placing one atom on top of Au_{16a}^- , whereas Au_{18b}^- can be viewed as placing one atom on top of Au_{17a}^- . Both Au_{17a}^- and Au_{18b}^- possess C_{2v} symmetry. At Au_{19}^- , there is only a single candidate for the lowest-energy structure, namely, Au_{19a}^- , whose energy is 0.2–0.3 eV lower (depending on the basis set) than the second-lowest-energy isomer (Au_{19b}^-) and ≈ 0.5 eV lower than the third-lowest-energy isomer (Au_{19c}^-). Au_{19a}^- exhibits a pyramidal structure, which is similar to the pyramidal Au_{20} (15) with one missing corner atom. This structural similarity is expected because Au_{19} is only one atom less than the highly stable (magic-number) pyramidal cluster Au_{20} (15). Compared

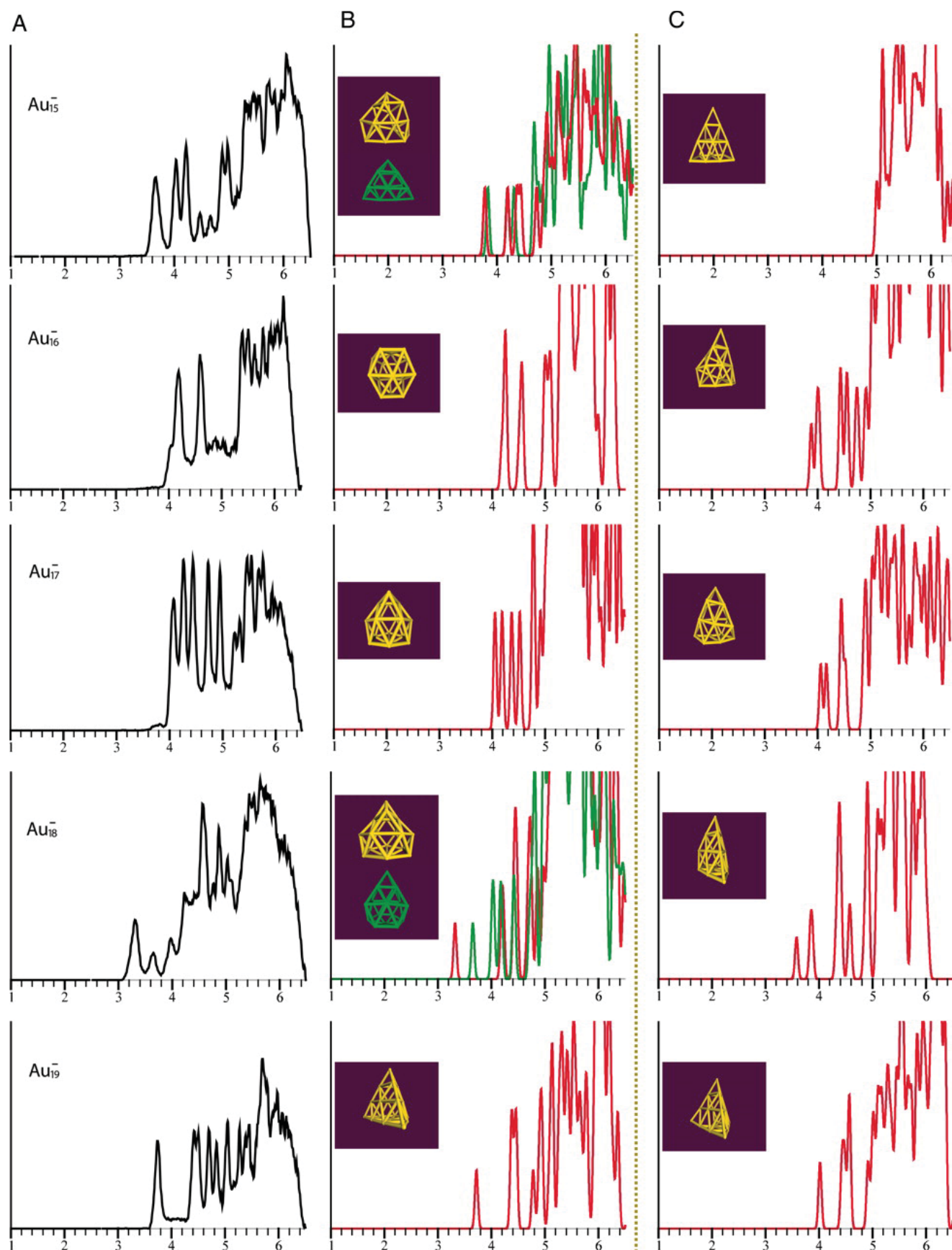


Fig. 1. Experimental photoelectron spectra of Au_n^- ($n = 15-19$) compared with those simulated theoretically. (A) Experimental spectra measured at 193 nm (6.424 eV). (B) The simulated spectra for one (or two) lowest-lying isomer that matches the first and second major peaks of the measured spectra. (C) The simulated spectra for the non-hollow-cage candidate isomer, which appears not to match the observed spectra.

Table 1. Experimental first VDEs for Au_n^- ($n = 15\text{--}19$) compared with computed values for the candidate lowest-energy clusters that give the best fit to the first two major peaks of the measured spectra

Isomer	VDE	
	Experimental	Theoretical
Au_{15a}^-	3.65 ± 0.03	3.777
Au_{16a}^-	4.03 ± 0.03	4.179
Au_{17a}^-	4.08 ± 0.03	4.053
Au_{18b}^-	3.32 ± 0.03	3.320
Au_{19a}^-	3.74 ± 0.03	3.720

All energies are in eV.

with Au_{19a}^- , the hollow-cage structures such as Au_{19c}^- and Au_{19d}^- are no longer energetically competitive (Fig. 4D). In other words, the structural transition from hollow-cage to pyramid-like structure appears to occur at Au_{19} . To illustrate the structural evolution of gold clusters from 2D planar to 3D flat-cage, hollow-cage, and pyramid-like structures, we highlight in Fig. 2 those candidate lowest-energy clusters that can provide reasonable match to the first two to four major peaks of the experimental photoelectron spectra (Fig. 1 A and B).

Our first-principles global search provides the electronic energy-based evidence that the overwhelming majority of the low-lying clusters of Au_{16}^- to Au_{18}^- exhibit hollow-cage structures. Moreover, our measured/simulated PES provides additional spectroscopic evidence to the existence of free-standing hollow golden cages. Here, we used the time-independent DFT (see *Methods*) to obtain approximated theoretical PES for all of the candidate lowest-energy structures of Au_{15}^- to Au_{19}^- (Figs. 1 and 3). Note also that the combined experimental and theoretical PES study has been used by many researchers to explore structures of small- to medium-sized clusters. This approach is particularly effective to identify structures of highly stable (magic-number) clusters such as the buckyball C_{60} or golden pyramid Au_{20} (15) because magic-number clusters are notably lower in energy than

other isomers (i.e., they are the undisputed lowest-energy cluster). In this sense, Au_{19a}^- , the sole candidate for the lowest-energy cluster of Au_{19}^- , can be viewed as a magic-number cluster because of the overwhelming stability of the pyramidal Au_{20} (15). As such, the simulated PES of Au_{19a}^- should match well with the measured one. Indeed, the location of the first two peaks near the threshold, which are directly related to the frontier orbitals and the VDE of the cluster, are in very good agreement with the measured one (including the weak doublet feature of the second major peak). Because the simulated PES based on DFT was obtained from the negatives of the Kohn–Sham (KS) eigenenergies (ground-state energy values), the simulated PES is not expected to match peak-for-peak with the measured PES beyond the threshold (energies of excited states). In summary, the location of the first two major peaks offers a critical structural “fingerprint” of the Au_{19a}^- . Conversely, the simulated PES for the second lowest-energy isomer (Au_{19b}^-), which is also pyramid-like, corresponding to the removal of an atom from the edge of the tetrahedral Au_{20} (15), does not agree with the experiment. The VDE of the first simulated peak is too high compared with the experiment (Fig. 1).

For other Au_n^- clusters ($n = 15\text{--}18$), each has five or six candidate lowest-energy structures (Fig. 4). Moreover, previous PES studies of the endohedral gold-cage cluster W@Au_{12} (19, 20) have shown that the gold cage is fluxional. In other words, the energy barriers separating structurally similar isomers (e.g., hollow cages) can be quite small. As a result, it is conceivable that multiple isomers may contribute to the experimental spectra. Hence, our first priority was to use the measured PES as a “filter” to identify those candidate isomers that cannot match the measured PES well (see Fig. 1C). Again, our main focus has been placed on the location of the first two major peaks and, to a lesser extent, the number of peaks in the 4- to 5-eV binding energy range. For example, at Au_{15} , the two pyramid-like low-lying isomers Au_{15c}^- and Au_{15e}^- can be ruled out (Fig. 3A). In fact, the simulated PES of the two flat-cage isomers Au_{15a}^- and Au_{15d}^- seem to match the measured PES (Fig. 1 A and B), particularly on the location of the two major peaks near the threshold.

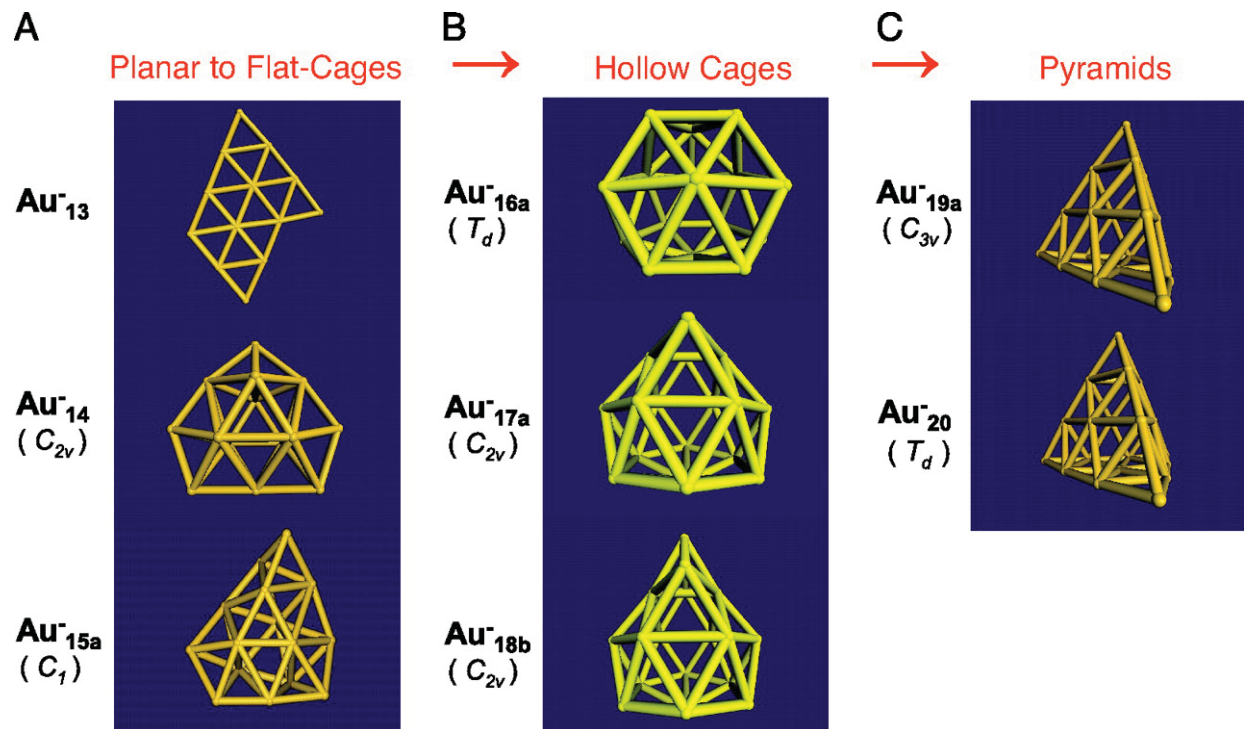


Fig. 2. Structural evolution of mid-sized gold anion clusters from Au_{13}^- to Au_{20}^- . (A) The 2D planar to 3D flat-cage structural transitions (11). (B) The hollow gold cages with diameters >5.5 Å. (C) The pyramid-like clusters, which resemble bulk gold (15).

At Au_{16}^- , the only non-hollow-cage isomer $\text{Au}_{16\text{c}}^-$ and the isomer $\text{Au}_{16\text{e}}^-$ can be ruled out because their first VDE seems to be lower than the experimental data (Fig. 3B). The remaining three isomers, $\text{Au}_{16\text{a}}^-$, $\text{Au}_{16\text{b}}^-$, and $\text{Au}_{16\text{d}}^-$, all give reasonable VDE, but $\text{Au}_{16\text{a}}^-$ seems to provide the best agreement with the experiment in term of the first two major peaks observed between 4 and 5 eV (Fig. 1B). Hence, $\text{Au}_{16\text{a}}^-$ is likely to be the most popular isomer in the mass-selected cluster beam. However, there are some weaker features in this binding energy range, suggesting the presence of other low-lying isomers (possibly $\text{Au}_{16\text{b}}^-$ and $\text{Au}_{16\text{d}}^-$) that may account for the observed weak features experimentally.

At Au_{17}^- , the measured PES spectrum displayed five relatively sharp and quite evenly separated peaks in between 4 and 5 eV (Fig. 1). On this ground, we can rule out the only non-hollow-cage isomer $\text{Au}_{17\text{c}}^-$ (Fig. 1C) and isomer $\text{Au}_{17\text{e}}^-$ among the six candidate lowest-energy structures. The simulated spectrum of $\text{Au}_{17\text{a}}^-$ seems to agree somewhat better than others with the observed spectral pattern. However, the simulated spectra of $\text{Au}_{17\text{b}}^-$, $\text{Au}_{17\text{d}}^-$, and $\text{Au}_{17\text{f}}^-$ (Fig. 3C) all have transitions in the same energy range so that they may coexist with the $\text{Au}_{17\text{a}}^-$ in the cluster beam. Note that all four hollow-cage isomers can be viewed as relaxed structures by placing an atom to the surface of the $\text{Au}_{16\text{a}}^-$ cage.

Lastly, at Au_{18}^- , it appears at first glance that none of the six candidate lowest-energy isomers can give good match with the measured PES (particularly the first two peaks). However, after a closer look we found that the simulated spectra of $\text{Au}_{18\text{b}}^-$ and $\text{Au}_{18\text{c}}^-$ match the first and fourth experimental peaks well (Fig. 1A and B), suggesting that the two relatively weak second and third experimental peaks were due to other isomers. Indeed, the simulated spectra of $\text{Au}_{18\text{a}}^-$, $\text{Au}_{18\text{d}}^-$, $\text{Au}_{18\text{e}}^-$, and $\text{Au}_{18\text{f}}^-$ all have transitions in the appropriate spectral range and may be candidates for these transitions. It is interesting to note that except $\text{Au}_{18\text{a}}^-$, all other low-lying isomers are hollow-cage structures, which can be viewed as placing an atom to the cages of Au_{17}^- . The only non-hollow-cage isomer, $\text{Au}_{18\text{a}}^-$, is pyramid-like, which can be viewed as removing two corner atoms from Au_{20}^- (15).

Overall, the fairly good agreement between the experimental and theoretical PES lends credence to the identified lowest-energy structures for the Au_n^- clusters ($n = 16\text{--}18$), which are predominately hollow cages. To date, all medium-sized metal clusters detected experimentally exhibit compact structures, a manifestation of the metallic effects due to delocalized electrons. The fact that anion gold clusters can form stable hollow cages in the mid-size range $n = 16\text{--}18$ is quite unusual. A natural question is why gold clusters favor hollow-cage structures in this special size range. Clearly, the strong relativistic effects and aurophilic attraction in gold must play a key role for the formation of the cages. In fact, a recent DFT study showed that copper clusters (a lighter noble-metal congener of gold) favor space-filling compact structures beyond the size $n = 16$ (21). Moreover, because of the lack of strong relativistic effects and aurophilic attraction in copper and silver, the 2D-to-3D structural transition occurs at $n = 7$ for both copper and silver anion clusters (22), whereas this transition occurs at $n = 14$ for gold anion clusters (10, 11). Hence, the formation of hollow gold cages in the size range of $n = 16\text{--}18$ reflects a compromise between the tendency of forming 2D planar structures at small sizes ($5 \leq n \leq 13$) and the tendency to form 3D compact structures at larger sizes ($n \geq 19$). At $n = 14$ and 15, the tendency of forming planar structures is stronger so that most low-lying clusters favor flat-cage structures. At $n = 16\text{--}18$, the hollow-cage structures seem to be the best compromise between the 2D and 3D structural competition, even though the pyramid-like compact structure starts to become energetically competitive at $n = 18$.

Finally, our preliminary calculations suggest that these hollow golden cages can easily accommodate a guest atom with very little structural distortion to the host cages. We note that an icosahedral Au_{12} cage with a central metal atom, M@Au_{12} , has been predicted

(19) and verified experimentally (20, 23). Recently, a larger gold cage with a central atom (M@Au_{14}) has been predicted to be very stable (24). However, bare Au_{12} and Au_{14} , as well as their anions, do not possess hollow-cage structures, and the endohedral cage structures M@Au_{12} and M@Au_{14} are mainly stabilized through the interaction between the central impurity atom M and the outer gold cage. The current mid-sized hollow golden cages with $n = 16\text{--}18$ suggest that a new class of novel endohedral gold clusters may exist, analogous to the endohedral carbon fullerenes with a metal inside (25, 26).

Methods

PES. The PES experiment was done similarly as for the smaller gold clusters (11) and Au_{20}^- (15). The gold cluster anions were produced by using a laser vaporization cluster source, and their PES spectra were obtained by using a magnetic-bottle time-of-flight photoelectron analyzer (27). Photoelectron spectra were measured at both 266 nm (4.661 eV) and 193 nm (6.424 eV) photon energies and calibrated with the known spectrum of Au^- .

Theoretical Calculations. We performed global-minimum searches using the basin-hopping method (12) for gold anion clusters Au_n^- in the size range $n = 15\text{--}19$. Here we combined the global search method directly with *ab initio* (relativistic) density-functional calculations (28). After each accepted Monte Carlo move, a geometry minimization was carried out. DFT calculations with a gradient-corrected functional [the Perdew–Burke–Ezerhof (PBE) exchange-correlation functional (29)] as implemented in the DMOL3 code (a density functional theory program distributed by Accelrys, Inc., San Diego; see ref. 30) were used for the geometric optimization from which the top-10 lowest-energy isomers were collected and listed in Fig. 4 (energy values in black). Among the top-10 isomers, those with their energy value within 0.2 eV from the lowest-energy isomer were all regarded as candidate lowest-energy structures to be compared with experimental data. Relative energies of these candidate isomers with respect to the lowest-energy isomer were further evaluated by using a modest (LANL2DZ) and a large [SDD+Au(2f)] basis set, respectively. The energy values shown in Fig. 4 (in blue color) are based on optimization with the PBEPBE/LANL2DZ functional/basis set, implemented in the GAUSSIAN 03 package (31), whereas the energy values in red color are based on single-point energy calculations at the PBEPBE/SDD+Au(2f)/PBEPBE/LANL2DZ level of theory, implemented in GAUSSIAN 03 package. Here “SDD+Au(2f)” denotes the Stuttgart/Dresden ECP valence basis (32, 33), augmented by two sets of *f* polarization functions (exponents = 1.425, 0.468). Finally, simulated anion photoelectron spectra (based on the DFT calculation with the PBEPBE/LANL2DZ functional and basis set) of all candidate lowest-energy isomers are shown in Fig. 3. Here, the first VDE was calculated as the energy of the neutral cluster at the geometry of the anion. Then the orbital energies from the deeper orbitals were added to the first VDE to give the density of states. Each peak was fitted with a Gaussian of width 0.04 eV to give the simulated anion photoelectron spectra presented. Details of the computational method to obtain simulated PES of gold clusters have been presented elsewhere (7, 11, 15).

Acknowledgements

We thank Profs. U. Landman, X. G. Gong, and A. I. Boldyrev and Drs. J. Li, S. Yoo, X. Wu, and J. Bai for valuable discussions. The theoretical work done at Nebraska was supported by Department of Energy (DOE) Office of Basic Energy Sciences Grant DE-FG02-04ER46164, the National Science Foundation (Division of Chemistry and Materials Research Science and Engineering Center), the John Simon Guggenheim Foundation, the Nebraska Research Initiative, and the University of Nebraska–Lincoln Research Computing

Facility. The experimental work done at Washington State was supported by National Science Foundation Grant CHE-0349426 and the John Simon Guggenheim Foundation; the work was performed at the Environmental Molecular Sciences Laboratory (a national scientific user facility sponsored by the DOE Office of Biological and Environmental Research, located at the Pacific Northwest National Laboratory, and operated for DOE by Battelle).

References

1. Kroto, H. W., Heath, J. R., O'Brien, S. C., Curl, R. F. & Smalley, R. E. (1985) *Nature* **318**, 162–163.
2. Kratschmer, W., Lamb, L. D., Fostiropoulos, K. & Huffman, D. R. (1990) *Nature* **347**, 354–358.
3. Bai, J., Virovets, A. V. & Scheer, M. (2003) *Science* **300**, 781–783.
4. Pyykkö, P. (2004) *Angew. Chem. Int. Ed* **43**, 4412–4456.
5. Johansson, M. P., Sundholm, D. & Vaara, J. (2004) *Angew. Chem. Int. Ed* **43**, 2678–2681.
6. Gu, X., Ji, M., Wei, S. H. & Gong, X. G. (2004) *Phys. Rev. B Condens. Matter* **70**, 205401-1–205401-5.
7. Ji, M., Gu, X., Li, X., Gong, X., Li, J. & Wang, L. S. (2005) *Angew. Chem. Int. Ed* **44**, 7119–7123.
8. Gao, Y. & Zeng, X. C. (2005) *J. Am. Chem. Soc* **127**, 3698–3699.
9. Wang, J., Jellinek, J., Zhao, J., Chen, Z., King, R. B. & Schleyer, P. V. R. (2005) *J. Phys. Chem. A* **109**, 9265–9269.
10. Furche, F., Ahlrichs, R., Weis, P., Jacob, C., Glib, S., Bierweiler, T. & Kappes, M. M. (2002) *J. Chem. Phys* **117**, 6982–6990.
11. Häkkinen, H., Yoon, B., Landman, U., Li, X., Zhai, H. J. & Wang, L. S. (2003) *J. Phys. Chem. A* **107**, 6168–6175.
12. Doye, J. P. K. & Wales, D. J. (1998) *New J. Chem* **22**, 733–744.
13. Wilson, N. T. & Johnston, R. L. (2000) *Eur. Phys. J. D* **12**, 161–169.
14. Wang, J., Wang, G. & Zhao, J. (2002) *Phys. Rev. B Condens. Matter* **66**, 035418-1–035418-6.
15. Li, J., Li, X., Zhai, H. J. & Wang, L. S. (2003) *Science* **299**, 864–867.
16. Olson, R. M., Varganov, R., Gordon, M. S., Metiu, H., Chretien, S., Piecuch, P., Kowalski, K., Kucharski, S. A. & Musial, M. (2005) *J. Am. Chem. Soc* **127**, 1049–1052.
17. Han, Y.-K. (2006) *J. Chem. Phys* **124**, 024316-1–024316-3.
18. Yoo, S. & Zeng, X. C. (2005) *J. Chem. Phys* **123**, 164303-1–164303-6.
19. Pyykkö, P. & Runeberg, N. (2002) *Angew. Chem. Int. Ed* **41**, 2174–2176.
20. Li, X., Kiran, B., Li, J., Zhai, H. J. & Wang, L. S. (2002) *Angew. Chem. Int. Ed* **41**, 4786–4789.
21. Yang, M., Jackson, K. A., Koehler, C., Frauenheim, T. & Jellinek, J. (2006) *J. Chem. Phys* **124**, 024308-1–024308-6.
22. Fernandez, E. M., Soler, J. M., Garzon, I. L. & Balbas, L. C. (2004) *Phys. Rev. B Condens. Matter* **70**, 165403-1–165403-14.
23. Zhai, H. J., Li, J. & Wang, L. S. (2004) *J. Chem. Phys* **121**, 8369–8374.
24. Gao, Y., Bulusu, S. & Zeng, X. C. (2005) *J. Am. Chem. Soc* **127**, 15680–15681.
25. Curl, R. F. & Smalley, R. E. (1988) *Science* **242**, 1017–1022.
26. Cai, Y., Guo, T., Jin, C., Haufler, R. E., Chibante, L. P. F., Fure, J., Wang, L., Alford, J. M. & Smalley, R. E. (1991) *J. Phys. Chem* **95**, 7564–7568.
27. Wang, L. S., Cheng, H. S. & Fan, J. (1995) *J. Chem. Phys* **102**, 9480–9493.
28. Yoo, S. & Zeng, X. C. (2005) *Angew. Chem. Int. Ed* **44**, 1491–1495.
29. Perdew, J. P., Burke, K. & Ernzerhof, M. (1996) *Phys. Rev. Lett* **77**, 3865–3868.
30. Delley, B. (1990) *J. Chem. Phys* **92**, 508–517.
31. Frisch, M. J., Trucks, G. W., Schlegel, H. B., Scuseria, G. E., Robb, M. A., Cheeseman, J. R., Montgomery, J. A. Jr., Vreven, T., Kudin, K. N. & Burant, J. C., *et al.* (2003) *GAUSSIAN 03 (Gaussian, Pittsburgh)* Revision C. 02.
32. Dolg, M., Wedig, U., Stoll, H. & Preuss, H. (1987) *J. Chem. Phys* **86**, 866–872.
33. Schwerdtfeger, P., Dolg, M., Schwarz, W. H. E., Bowmaker, G. A. & Boyd, P. D. W. (1989) *J. Chem. Phys* **91**, 1762–1774.